Fiber optic refractive index sensing using an inline dual semi-distributed interferometer

Alina Adilkhanova [a,b], Marzhan Nurlankyzy [a,c], Sakengali Kazhiyev [c], Wilfried Blanc [d], Aliya Bekmurzayeva [a,*], Daniele Tosi [a,c]

[a] Laboratory of Biosensors and Bioinstruments, National Laboratory Astana, Nazarbayev University, Astana, Kazakhstan
[b] School of Sciences and Humanities, Nazarbayev University, Astana, Kazakhstan
[c] School of Engineering and Digital Sciences, Nazarbayev University, Astana, Kazakhstan
[d] INPHYNI, CNRS UMR7010, Université Côte d'Azur, Nice, France

ARTICLE INFO

Keywords:
Refractive index sensor
Optical fiber sensor
Fabry-Perot interferometer
High-scattering fibers
Optical fiber refractometer
Vernier effect

ABSTRACT

In this work, we present a fiber optic refractive index (RI) sensor based on a dual inline semi-distributed interferometer (SDI) device. The SDI is formed within a telecom-grade optical fiber by simply splicing a short length of a high-scattering fiber; the presence of a high density of scattering centers induces a distributed cavity effect, forming a low-finesse interferometer. Here, we propose an approach based on two serial SDIs, with few millimeters spacing between the two cavities; the outer SDI encodes the changes of surrounding RI, while the inner probe is RI-insensitive and can be used as a reference. Experimental analysis shows that the dual-SDI device has RI sensitivity of 111.2–466.2 dB/RIU with RI-sensitive mode, and 0.4–3.7 dB/RIU with RI-insensitive mode, with a ratio up to 1165.5 between sensitive and insensitive modes. In addition, the Vernier effect can be interrogated by detecting the wavelength shift of the narrow spectral lines, with sensitivity of 0.303 nm/RIU.

The dual-SDI structure maintains the same fabrication ease of a single SDI, since all process is made through splicing and cleaving fibers with a telecom-grade fiber. The key advantage is the availability of modes having both high and near-zero RI sensitivity, which therefore can be used for a referenced RI detection as an *in-situ* probe.

1. Introduction

The measurement of refractive index (RI) is an important asset in the field of sensing, particularly through the use of compact and miniaturized devices. The RI is a constitutive parameter of materials and defines its electromagnetic properties, and particular the speed of light propagation into the medium. In general, refractometers measure the RI variation from a baseline value [1]; in modern sensing systems they play a substantial role, particularly for the analysis of gases [2] (where RI ≈ 1), and aqueous media (RI ≈ 1.33) [3]. The latter is of particular importance for the development of label-free biosensors [4], in which a refractometer is subsequently functionalized by means of silanization or nanomaterial layers [5] with the addition of bioreceptors to bind to a target biomolecules resolving their concentrations [6].

Fiber-optic technologies are an excellent candidate for the RI sensors, as they allow the realization of intrinsic or extrinsic probes

* Correspondence to: 53 Kabanbay batyr avenue, Astana 010000, Kazakhstan.
E-mail address: abekmurzayeva@nu.edu.kz (A. Bekmurzayeva).

capable of sensing the RI changes surrounding the fiber [7]. Several methods have been presented for RI sensing using large-core multimode fibers, typically using surface plasmon resonance [8] or lossy mode resonance [9] effects in metallic or 2D materials [10], as well as U-bent fiber shapes [11], and inline tapered sensors labeled as Waveflex [12,13], and combinations of inline tapers and plasmonic effects [14]. Other methods make use of single-mode telecom-grade fibers for the RI detection [15]: such devices either maintain single-modality over the whole propagation length, for example using ball-tip resonators [16], exposed core fibers [17], or tapers [18], or using a single-mode fiber to excite cladding modes such as in tilted fiber Bragg gratings and in long-period gratings [3], with the possibility of etching the fiber to control the cladding modes sensitivity [19,20].

Interferometry is another popular method for RI sensors having high performance; all-fiber interferometers reproduce in an optical fiber the free-space interferometric configurations, such as Mach-Zehnder [21], Fabry-Perot [22], or Sagnac [23], whereas the resulting spectrum is a result of interfering waves propagating along multiple optical paths.

The most popular way to design an RI-sensitive fiber-optic interferometer is to manipulate the structure of the fiber such that the RI changes affect the optical path length along one or multiple branches of the interferometer. Since the free spectral range of the interferometer varies with the changes of the optical path length, this method allows the realization of high-sensitivity RI sensors and biosensors that translate the RI changes into wavelength shift of spectral features, such as spectral peaks or valleys [24]. This method is at the base of several interferometric schemes relying on core-exposed microfibers [25,26], harmonic gratings [27], tapered or knotted microfibers [28,29], modal interferometers [30,31] among others.

These structures, despite the high sensitivity often exceeding the 10,000 nm/RIU figure [32], require a complex fabrication process to manipulate the microfiber, and often lead to a very fragile structure due to the thin diameter which hampers the surface-functionalization processes; in addition, most of these sensors work in transmission. Thus, recent studies have focused on much simpler interferometric structures that encode the RI changes into the variation of reflectivity observed on the fiber tip; then, a Fabry-Perot cavity is fabricated by means of splicing a short fiber section that introduces a mirror-like reflectance within the fiber propagation path. Such systems have been presented by Zhu et al. [33], labeled as supermode interferometer and using a multicore fiber as a cavity, and by Rakhimbekova et al. [34], defined as semi-distributed interferometer (SDI) and using a nanoparticle-doped fiber with enhanced scattering to provide an interferometric spectrum. These approaches have an extremely simple splice-and-cleave fabrication type with telecom-grade splicers; they encode the RI changes into variations of the intensity of each spectral peak/valley, with estimated sensitivity up to 787 dB/RIU [24].

One of the main drawbacks of the sensing devices based on SDI or supermode interferometers is that all the modes of the interferometer are RI-sensitive; in a practical application, users might not be able to disambiguate the spectral changes due to surrounding RI variations from the power fluctuations occurring in the system (for example, the power drifts of a laser source).

In this work, we introduce a dual inline SDI configuration, formed by cascading two SDI interferometers interleaved by a short single-mode fiber section. The overall structure behaves as a combination of two interferometers, whereas the inner one does not sense RI changes and the outer one is RI-sensitive. While the fabrication process remains simple, and based on the same splice-and-cleave approach of a single SDI [24], the dual-SDI structure provides modes that are both sensitive and insensitive to the RI and introduces the Vernier effect [35].

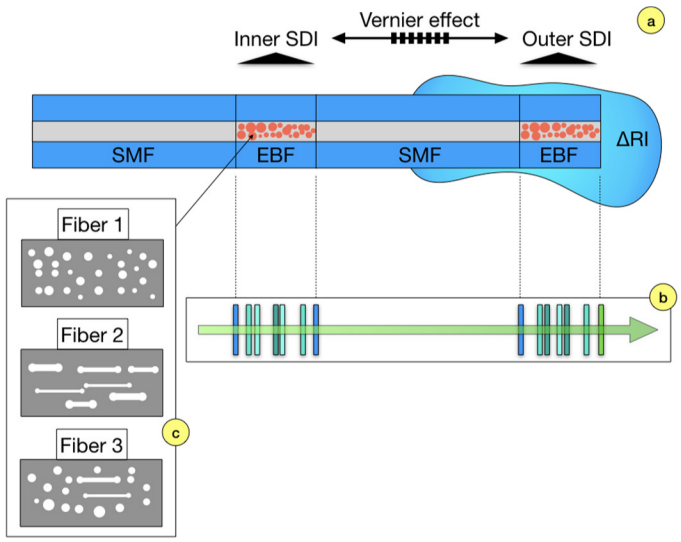

Fig. 1. Schematic of the dual-SDI probe formed by two inline SDI interferometers. (a) Schematic of the sensor; (b) equivalent electromagnetic model, formed by cascades of random mirrors with random reflectivity and spacing; (c) sketch of the types of graphic core defects forming the enhanced backscattering fibers.

2. Working principle and setup

2.1. Working principle

The working principle of the SDI is sketched in Fig. 1. A single SDI is an interferometer that resembles the Fabry-Perot cavity, and is formed at the interface between an enhanced backscattering fiber (EBF) and a single-mode fiber (SMF) [34]: the small reflection occurring at the EBF/SMF interface form a low-reflective mirror, that acts as one side of the cavity. In a dual-SDI, we exploit two SDI cavities, one inner cavity formed by a SMF-EBF-SMF structure and entirely included within the propagation path, and one external cavity formed by SMF/EBF interface and an external mirror, formed by the Fresnel reflection between the cleaved EBF and the outer medium. The EBF fibers here play dual functions: (1) a beneficial role forming a weak mirror when interfaced with a SMF, which simply by splicing allows forming one side of a Fabry-Perot cavity; (2) due to the inner and random reflections, produce an additional random phase shift in each fiber section, which causes the resulting spectra to randomize the spectral envelope. The ΔRI changes occurring at the outer mirror cause variations of the reflection coefficient of the rightmost mirror of the interferometer.

Fig. 1(b) shows the electromagnetic model of the dual-SDI probe, whereas we convert each element of the system into its equivalent transmission matrix. The inner SDI is formed by two external mirrors formed at each SMF/EBF interface, each with reflectivity $\sim 10^{-5}$ that can be measured on the analyzer [36]; the high concentration of scattering centers induces a distributed set of reflections, that act as a series of mirrors with random reflectivity and spatial distribution. The outer interferometer has a similar pattern, with the external mirror formed as the RI-dependent Fresnel reflection between the fiber and the surrounding medium. The SMF fiber that separates the SDIs forms a further cavity between the two interferometers, which introduces an inline Vernier effect [37] that modulates the spectra of both interference fringes. The dual-SDI probe has been validated using different types of EBF, drawn with different parameters and having multiple types of scattering defects within the fiber core; a scanning electron microscopy (SEM) view of the inner portion of the fiber core for fibers drawn in similar conditions is reported in [38].

2.2. Fabrication of the dual-SDI probe

The fabrication process for the dual-SDI sensor is shown in Fig. 2. All the process takes place by splicing SMF fibers (Corning SMF-28e+) and EBF fibers, customized with the core doped with a high density of nanoparticles in order to substantially increase the backscatter signal over 5 orders of magnitude [39]. The entire process has been carried out by means of telecom-grade splicer and cleaver (Fujikura 12-S) using SMF-SMF splicing protocol. The first SMF was spliced to an EBF, which was then cleaved and spliced to a further SMF span to form the inner SDI. This section was subsequently spliced to a second EBF, which was then cleaved on the tip to form the Fresnel reflection.

This process allows a simple fabrication, with duration of few minutes and using all telecom-grade splicing methods. Due to the manual cleaving process, the operator cannot set the length of each of the two SDIs and the SMF fiber that spaces the two cavities. In addition, the random nature of the scattering defect within each EBF induces stochastic reflective patterns within each SDI cavity.

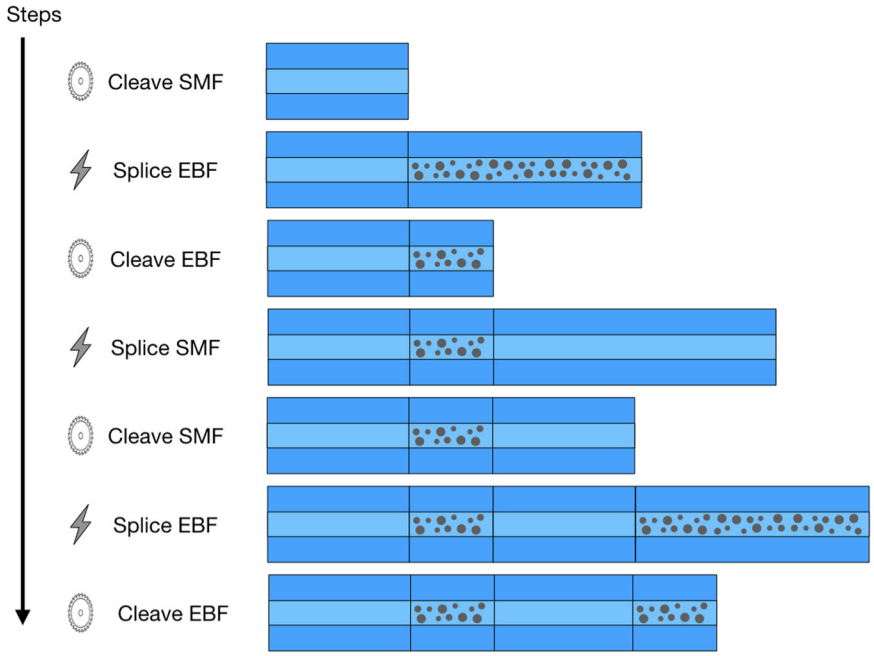

Fig. 2. Fabrication process for the dual-SDI probe.

The fabrication of the EBF fibers was carried out according to previous works [38]. To obtain the fiber, first a preform was prepared based on the Modified Chemical Vapor Deposition (MCVD) process [40]. A silica porous layer doped with germanium was deposited inside the silica substrate tube. Lanthanum ions were incorporated in the core through the solution doping step. 0.7 mol/l of $LaCL_3$were dissolved in ethanol. Then the solution was removed and the tube was collapsed to form the preform. The diameter of the core is 0.8 mm (external diameter: 9.6 mm). Its refractive index cannot be measured due to the high scattering induced by the La-silicate nanoparticles (the preform core is white). This preform was drawn at three different temperatures and two different drawing speed: 2050 °C (21 m/min), 1950 °C (21 m/min) and 1800 °C (32 m/min). The fiber core diameter is (about 10 μm (external diameter of the fiber is 125 μm).

In order to analyze the behavior of the dual-SDI probes with different types of defects, three sensors have been fabricated using different drawing parameters, as shown in Fig. 3. The first fiber has been drawn at 21.3 m/min speed at 2050 °C, which forms smaller defects within the fiber core. The second and third fibers have been drawn at 21.3 m/min speed at 1800 °C, and at 32 m/min speed at 1950 °C respectively; these fibers form more elongated defects within the fiber core. The scattering parameters of the fibers, listed in Fig. 3(b-c), have been measured using an optical backscatter analyzer (OBR). All three fibers have similar scattering gain (55.6 – 60.3 dB), defined as the increment in scattering of the EBF with respect to a standard SMF [41]. The two-way attenuation values differ substantially between the first fiber (0.04 dB/mm) and the other two fibers (1.37–1.84 dB/mm), due to the different impact of the scattering defects [24].

2.3. Interrogation and calibration of the sensor

Experimental results have been carried out using an OBR analyzer (Luna OBR4600), operating on the telecom wavelength range (1535–1610 nm). RI measurements have been performed by using different sucrose mixtures, with refractive index ranging from 1.34761 to 1.35845; this small signal analysis, operating on a RI range of 10.84×10^{-3} RIU (refractive index units) in steps of $\sim 2.1 \times 10^{-3}$ RIU mimics the operation of fiber-optic biosensors in aqueous media, where changes in surrounding RI of $10^{-3} - 10^{-2}$ RIU are observed [3].

The double-inline-interferometer structure of the dual-SDI probe enables multiple methods for the interrogation, as illustrated in Fig. 4. A first method relies on the spatial discrimination capability of the OBR, or a generic optical frequency-domain reflectometer (OFDR) [42,43]. On the OBR, the spectral detection can be split by separately interrogating the outer SDI, which encodes the RI sensitivity, and the inner SDI which is insensitive to the RI and can be used as a reference (for example, to estimate drifts of the light source or temperature variations [44]). This method can be only achieved with an OFDR source, and has the drawback of possible crosstalk between the two interferometers.

The second method can be implemented with any spectral analyzer, such as an optical spectrum analyzer or a fiber Bragg grating interrogator. In this approach, the whole spectrum of the dual-SDI probe is detected, which includes a plurality of modes with regular periodicity, overlapped to the spectral comb due to the Vernier effect [35]. The spectral comb can be mitigated using a low-pass filter that extracts the envelope from the overall spectrum; in this work, we employed a digital Butterworth filter (5 taps, cut-off 0.02). The obtained envelope contains several modes each having various RI sensitivity ratings, and therefore we can obtain modes having either high or negligible RI sensitivity to be use for sensing or for reference, respectively.

A third method instead focuses on the interrogation of the wavelength shift, applied to the spectral comb due to the Vernier effect, due to the phase shift of the reflection coefficient of the outer interferometer [45]. In this way, the spectral comb appears to have a small wavelength shift, which can be estimated using a fitting method [46].

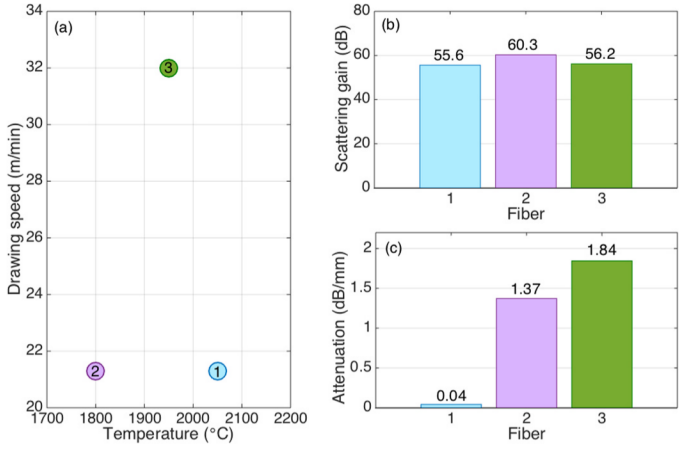

Fig. 3. Parameters of the three EBF fibers used for the dual-SDI probes. (a) Drawing parameters (speed, temperature) of the fibers; (b) Scattering gain for each fiber; (c) Two-way fiber attenuation values.

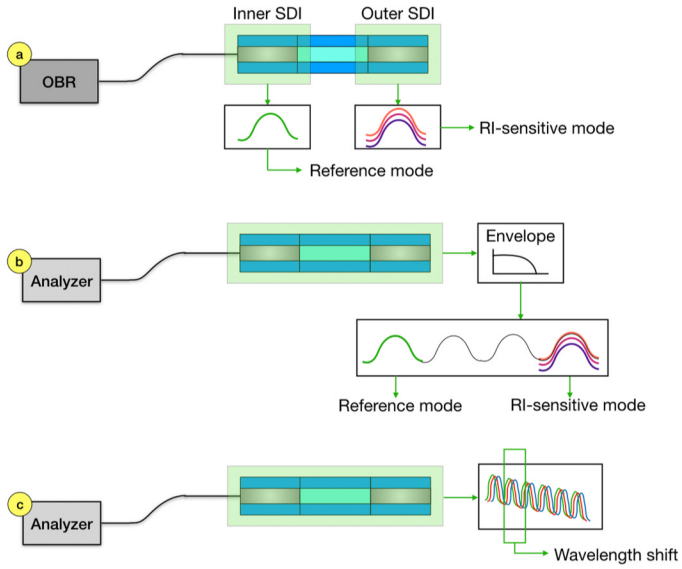

Fig. 4. Interrogation methods proposed for the dual-SDI probe. (a) OBR-based methods, interrogating each interferometer separately; (b) Spectral analysis, using a low-pass to extract the envelope of the dual-SDI probe; (c) Spectral analysis, interrogating the wavelength shift obtained in the Vernier effect.

3. Experimental results

Fig. 5 shows the spectra of a dual-SDI sensor, providing an assessment on the spectrum of the device in reference RI condition. The inner SDI displays an interferometric-like spectrum, similar to the one observed in [24] and characterized by several modes having free spectral range up to about 10 nm. The return loss ranges between −78 dB and −43 dB, while the distributed reflections occurring

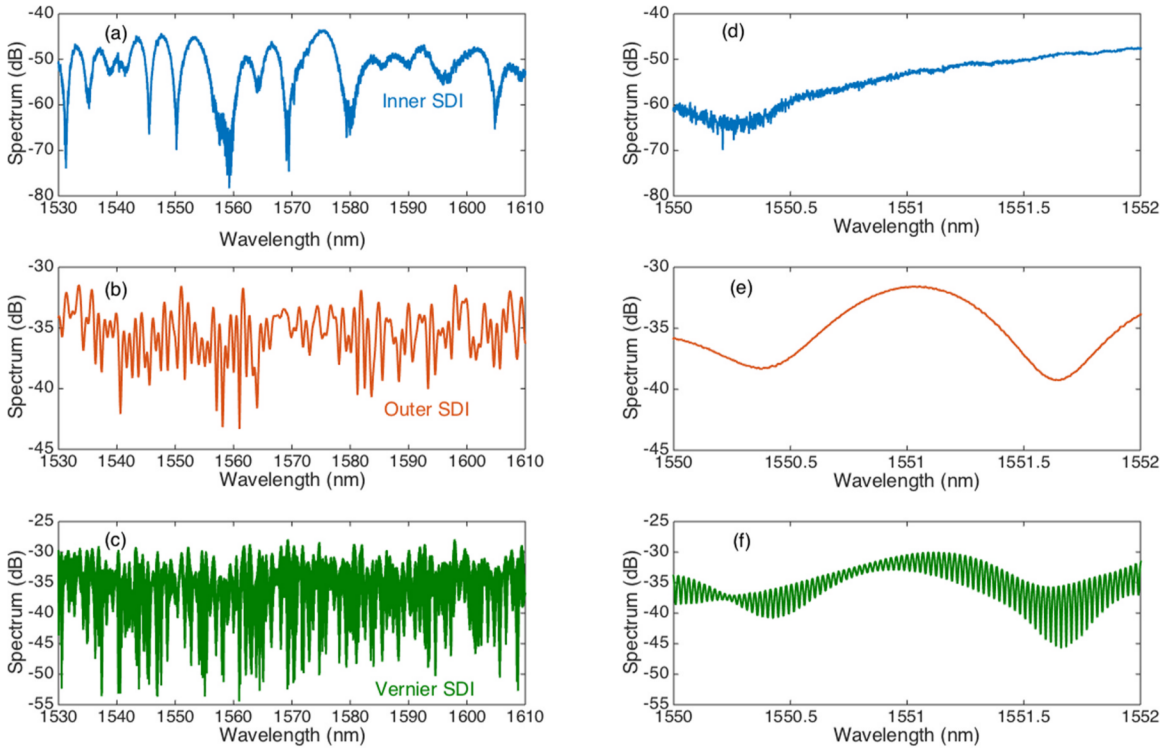

Fig. 5. Reflection spectra of a dual-SDI probe, obtained by individually interrogating (a) the inner SDI, (b) the outer SDI, and (c) integrating the whole probe visualizing the Vernier effect (d-f) Insets on a spectral portion with 2 nm width.

within the EBF fiber result in a quite chaotic envelope of the reflection spectrum. The outer SDI, fabricated with the same fiber, has a higher return loss (-43 dB to −31 dB), due to the fact that the external mirror has a much higher reflectivity with respect to an EBF/SMF interface; the spectrum appears with a quasi-periodical pattern, with a different pitch that is due both to the length of the EBF span and to the reflection pattern within the fiber.

When interrogating the whole spectrum of the dual-SDI, the Vernier spectrum appears; this can be well visualized in the Fig. 5(f), where we observe the envelope of the spectrum modulated by a comb with 23 pm width between each peak/valley. The envelope of the whole spectrum results as a combination of the two interferometers, obtaining a resulting modulation of the intensity of each peak/valley.

The effect of RI sensitivity on each element of the dual-SDI can be observed in Fig. 6, which displays the spectra of inner and outer interferometer, as well as the envelope of the dual-SDI spectrum, for two different RI values. The spectrum of the inner interferometer is independent on RI, as the two spectra are almost perfectly overlapping over the whole wavelength range of analysis. The outer interferometer, on the other hand, displays a plurality of modes each having a positive or negative RI sensitivity, as observed in [24]. The dual-SDI spectrum, obtained by low-pass digital filtering the overall spectrum, results in a combination of the previous spectra; the RI sensitivity is well visible in the dip around 1555 nm, but the surrounding peaks do not feature any perceivable RI sensitivity.

The RI sensitivity for a dual-SDI probe can be visualized in Fig. 7, which reports the spectra for the probe fabricated with the fiber 1 for 6 values of refractive index. The spectrum displays a dense set of peaks and valleys, with RI sensitivity that appears different for each spectral feature. This can be observed for some features in Fig. 7(b), where we see the rightmost spectral peak with a steep RI sensitivity, while the other three peaks have RI sensitivity that appears significantly inferior. The sensitivity to RI can be estimated from each peak or valley, as shown in Fig. 7(c) whereas the intensity for each peak is reported as a function of RI. Due to the reduction of the Fresnel reflection at the interface between the fiber and the outer medium, the increase of RI causes a reduction of the reflection spectrum that has a high linearity ($R^2 > 0.95$). Each spectral feature can be determined using a peak extraction method, with sensitivity up to 171 dB/RIU.

Fig. 8 reports the RI sensitivity observed for the inner SDI, the outer SDI, and the dual-SDI after eliminating the Vernier comb with low-pass filtering; this interrogation mimics the spectral analysis that can be performed on OFDR or OBR analyzers. The inner SDI is insensitive to the RI, with only one peak having a visible RI sensitivity (possibly due to cross-talk in the OBR traces), with median sensitivity below 5 dB/RIU. When integrating only the outer SDI, we observe sensitivity values up to 261.0 – 713.5 dB/RIU depending on whether we detect peaks or valleys in the spectrum; these results are consistent with previous works using high-scattering fibers with elongated defects [24]. The dual-SDI analysis shows several modes with sensitivity >100 dB/RIU, but the median mode has low RI sensitivity and therefore the spectrum contains both high and low sensitivity to RI.

In practical applications, interrogators such as Fiber Bragg grating analyzers or grating-based spectrometers with coarser resolution are employed, having cost and portability more affordable with respect to bulky OBR systems [46]. Besides the lack of spatial resolution, these analyzers have a narrower dynamic range and a higher noise floor, which results in the spectral dips have a lower visibility over the noise floor. Hence, in order to evaluate the performances of a dual-SDI probe in a real-case scenario, we focus on the detection of only the spectral peaks over the dual-SDI spectrum that can be detected with >2 dB prominence.

This analysis is reported in Fig. 9, which reports the sensitivity ratings for each of the three dual-SDI probes. For the first fiber, the maximum RI sensitivity is 135.6 dB/RIU, while the lowest one is 0.7 dB/RIU, while the average sensitivity is 35.5 dB/RIU. For the second fiber, the maximum sensitivity is 556.6 dB/RIU, the lowest sensitivity is 0.1 dB/RIU, while the average sensitivity is 4.1 dB/RIU. For the third fiber, the maximum sensitivity is 244.8 dB/RIU, the lowest sensitivity is 1.2 dB/RIU, while the average sensitivity is 28.5 dB/RIU.

A good metric to evaluate the reliability in RI detection is to take into account the average of the 5 highest RI-sensitive modes (H5),

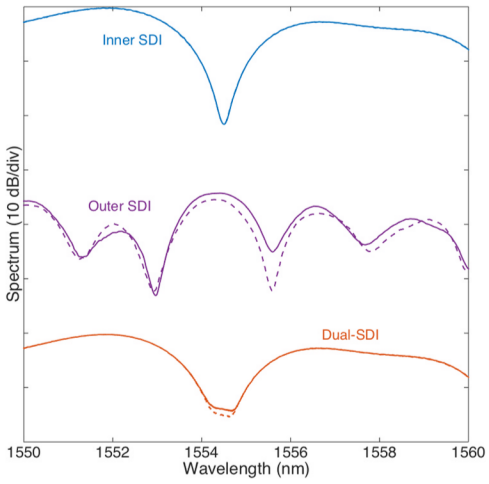

Fig. 6. Reflection spectra the inner, outer, and dual-SDI interferometer fabricated with the fiber 3. Vertical axis is normalized (10 dB/division). Solid line = reference spectrum, dashed line = spectra observed for RI increment of 10.84×10^{-3} RIU.

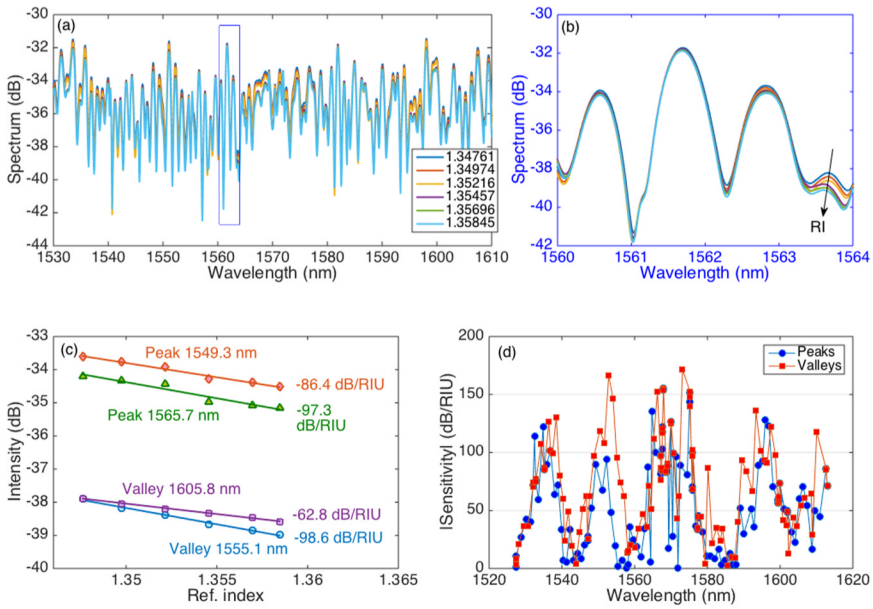

Fig. 7. Sensitivity to refractive index for a dual-SDI probe, fabricated with the first fiber. (a) Reflection spectrum of the probe. (b) Inset on a spectral portion of 4 nm, displaying the RI sensitivity. (c) RI sensitivity for 4 spectral features (peaks and valleys), extracted from the overall spectrum. (d) RI sensitivity displayed for all spectral features (peaks and valleys) extracted from the overall spectrum.

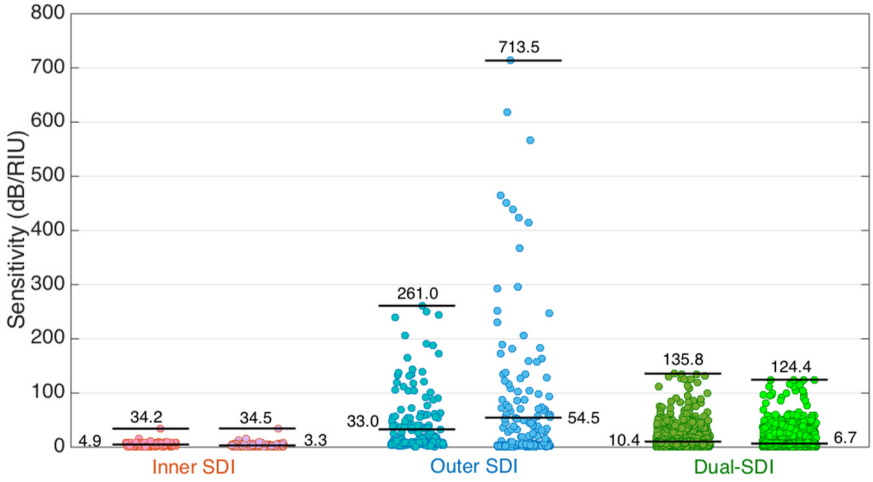

Fig. 8. RI sensitivity for each mode detected within the dual-SDI interferometer. Each data point reports the sensitivity observed for a different peak (left) and valley (right). The markers report the maximum and the median values.

and the average of the 5 modes that have the lowest sensitivity (L5) and can be used as a reference. For the first fiber, we have H5 = 111.2 dB/RIU and L5 = 3.7 dB, with H5/L5 = 30.1; for the second fiber, H5 = 466.2 dB/RIU, L5 = 0.4 dB/RIU, and H5/L5 = 1165.5; for the third fiber, H5 = 148.4 dB/RIU, L5 = 2.6 dB/RIU, H5/L5 = 57.1.

These values show that the RI performances appear superior for the second fiber, drawn at the lowest temperature and characterized by elongated defects within the fiber core. In this fiber we record the highest sensitivity to RI, but also a plurality of modes that are almost RI-insensitive; in fact, looking at the sensitivity data points, the modes are almost perfectly split between modes with high RI sensitivity (>50 dB/RIU) and modes with negligible sensitivity (<4 dB/RIU), whereas in the other fibers the distribution of the sensitivity values across each mode appears more regular.

For all the dual-SDI sensors it is however possible to guarantee the RI sensitivity with a reference system, since all sensors have a sensitivity >100 dB/RIU (much higher than simple Fresnel effect [47] or other inline Fresnel-based Fabry-Perot interferometers [33], while having a plurality of well-detectable modes with low sensitivity that can serve as a reference, for example to compensate laser power drifts over long operations.

Looking at possible biosensing applications, we can evaluate the impact of the presence of high and low sensitivity to RI. A case

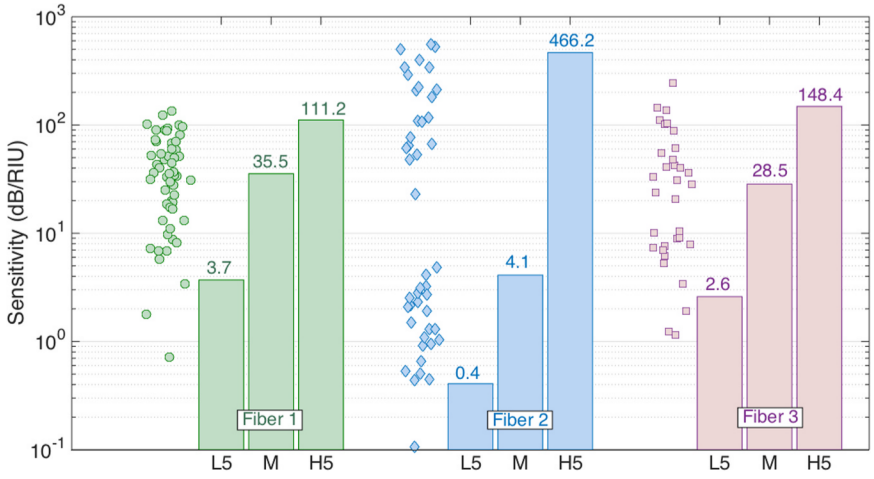

Fig. 9. Sensitivity for the dual-SDI probes, estimated in all the peaks having >2 dB prominence. For each fiber, the chart reports the sensitivity of each mode (data points), the average of the 5 modes having the lowest sensitivity (L5), the mean sensitivity (M), and the average for the 5 modes having the highest sensitivity (H5).

scenario might be considered the detection of CD44 cancer biomarker [4], where the RI change is 0.014 RIU from the blank sample to the highest concentration. Using the H5 metric, this RI interval would correspond to 1.55 dB, 6.52 dB, 2.08 dB for each of the three fibers; the RI-insensitive mode, for the same RI change would detect a fluctuation of 0.05 dB, 0.01 dB, 0.04 dB, which is compatible with the noise floor of the interrogator (~0.02 dB). Similar considerations can be drawn for low-contrast proteins such as thrombin [48]. This confirms that the L5 metric can be used for power compensation, or thermal detection.

Looking at other intensity-varying biosensors based on SMF fibers, the obtained sensitivity ratings of 111.2 dB/RIU up to 466.2 dB/RIU intersect the values recorded for other RI sensors such as ball resonators (256.0 – 566.2 dB/RIU [49]) and polarization-resolved ball resonators (366.6 – 6691.6 dB/RIU [16]), single-SDI fabricated with MgO nanoparticles (92.5 dB/RIU [34]) and silica nanoparticles (71.6 – 787.0 dB/RIU [24]).

Finally, we show in Fig. 10 the direct interrogation of the Vernier effect, which consist in the detection of the wavelength shift for the overall reflection spectrum without extracting its envelope. The spectrum is characterized by densely packed modes, due to the resonances between the inner and outer cavities, in which we observe a wavelength shift due to the phase variation in the reflection coefficients as a function of the external RI. When the RI increases, we observe a detectable shift towards shorter wavelengths, with slope of 303 pm/RIU. The sensitivity is however low, and is hard to estimate due to the resolution of the analyzer, and therefore this interrogation can be hardly applied experimentally; besides it can also be affected by the temperature sensitivity (~10 pm/°C as estimated in [44]). In this configuration, the Vernier effect does not contribute to increase the sensing performances in substantial way, but it rather can be simply removed by using a digital low-pass filter.

4. Conclusions

In conclusion, we proposed a dual-SDI sensor for refractive index detection, having a very simple splice-and-cleave fabrication process entirely based on telecom-grade splicers. The sensor is formed by cascading two semi-distributed interferometers; the working principle is similar to a Fabry-Perot interferometer with each in-fiber mirror formed by the interface between a single-mode fiber and an enhanced backscattering fiber, and an outer mirror formed by a fiber cleave.

The spectrum of a dual-SDI combines the envelope of both SDI interferometers, and is modulated by the mode comb due to the Vernier effect. The interrogation can be performed either detecting each interferometer separately exploiting the OFDR principle, or by interrogating the envelope of the overall reflection spectrum (as on most of the spectral analyzers). Unlike a single SDI, in which the RI sensitivity is encoded in every spectral feature, the spectrum of the dual-SDI is characterized by features having high sensitivity as well as spectral features with negligible RI sensitivity.

Three dual-SDI probes have been manufactured, varying the type of scattering defects within the fiber core. The best results have been obtained with a fiber with elongated defects, achieving sensitivity up to 466.2 dB/RIU (average of the 5 most sensitive spectral peaks), while low-sensitivity features have sensitivity of 0.4 dB/RIU, over 1000 times less sensitive. The other probes achieve sensitivity of 111.2 dB/RIU and 148.4 dB/RIU, with RI-insensitive features having ratings of 3.7 dB/RIU and 2.6 dB/RIU.

The dual-SDI probe, similarly to other inline interferometers, can be used both as refractometer for highly sensitive RI detection, as well as for biosensing thanks to the high sensitivity in aqueous media and the possibility to host bioreceptors on the fiber tip. In practical applications, the fact that the spectrum encompasses both RI sensitive and insensitive features provides a key advantage: as the main vulnerability of intensity-based detection is the low tolerance to spectral offset (due for example to power drifts of the light source), the dual-SDI provides a robust detection in which the differential between the RI-sensitive peaks and the reference peaks can be estimated, achieving a more reliable RI detection. In practical applications, the dual-SDI probe achieves a two-fold advantage with

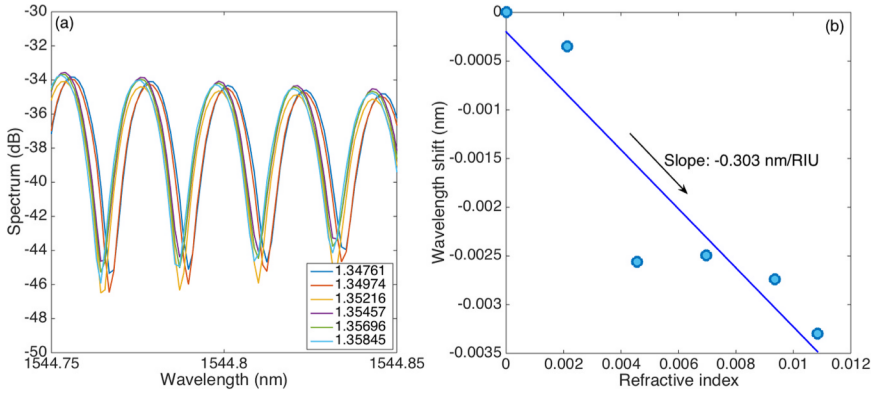

Fig. 10. Estimation of the wavelength shift sensitivity in the interrogation of the Vernier-effect comb. (a) Inset on a spectral portion of 100 pm for the dual-SDI spectrum; (b) Estimation of the wavelength shift as a function of the RI for the mode at 1544.8 nm wavelength ($R^2 = 0.85$).

respect to other SMF-based biosensors: 1) Ease of fabrication, as each sensor has a fabrication process that lasts a few minutes only and can be scaled, since only a telecom splicer is used; 2) Encode the RI sensitivity in few spectral features, with the other spectral features that can be used as reference, for example for temperature estimation or for compensating the drifts of the laser source.

Funding

This research has been funded by the Science Committee of the Ministry of Science and Higher Education of the Republic of Kazakhstan (Grant No. AP19576207), and by Nazarbayev University grant, code: 20122022FD4134 (Project M2O-DISK).

CRediT authorship contribution statement

Daniele Tosi: Writing – review & editing, Writing – original draft, Supervision, Software, Funding acquisition, Formal analysis, Data curation, Conceptualization. **Wilfried Blanc:** Writing – review & editing, Resources, Investigation. **Aliya Bekmurzayeva:** Writing – review & editing, Supervision, Investigation, Funding acquisition. **Marzhan Nurlankyzy:** Methodology, Investigation. **Sakengali Kazhiyev:** Software, Methodology, Investigation. **Alina Adilkhanova:** Writing – review & editing, Software, Methodology, Investigation, Formal analysis.

Declaration of Competing Interest

The authors declare that they have no known competing financial interests or personal relationships that could have appeared to influence the work reported in this paper.

Data Availability

Data will be made available on request.

References

[1] S. Singh, Refractive index measurement and its applications, Phys. Scr. 65 (2002) 167–180, https://doi.org/10.1238/Physica.Regular.065a00167.
[2] C. Caucheteur, T. Guo, F. Liu, B.-O. Guan, J. Albert, Ultrasensitive plasmonic sensing in air using optical fibre spectral combs, Nat. Commun. 7 (2016) 13371, https://doi.org/10.1038/ncomms13371.
[3] F. Chiavaioli, C. Gouveia, P. Jorge, F. Baldini, Towards a uniform metrological assessment of grating-based optical fiber sensors: from refractometers to biosensors, Biosensors 7 (2017) 23, https://doi.org/10.3390/bios7020023.
[4] A. Bekmurzayeva, Z. Ashikbayeva, N. Assylbekova, Z. Myrkhiyeva, A. Dauletova, T. Ayupova, M. Shaimerdenova, D. Tosi, Ultra-wide, attomolar-level limit detection of CD44 biomarker with a silanized optical fiber biosensor, Biosens. Bioelectron. 208 (2022) 114217, https://doi.org/10.1016/j.bios.2022.114217.
[5] M. Li, R. Singh, Y. Wang, C. Marques, B. Zhang, S. Kumar, Advances in novel nanomaterial-based optical fiber biosensors—a review, Biosensors 12 (2022) 843, https://doi.org/10.3390/bios12100843.
[6] C. Leitão, S.O. Pereira, C. Marques, N. Cennamo, L. Zeni, M. Shaimerdenova, T. Ayupova, D. Tosi, Cost-effective fiber optic solutions for biosensing, Biosensors 12 (2022) 575, https://doi.org/10.3390/bios12080575.
[7] J. Li, A review: Development of novel fiber-optic platforms for bulk and surface refractive index sensing applications, Sens. Actuators Rep. 2 (2020) 100018, https://doi.org/10.1016/j.snr.2020.100018.
[8] A.K. Sharma, R. Jha, B.D. Gupta, Fiber-optic sensors based on surface plasmon resonance: a comprehensive review, IEEE Sens. J. 7 (2007) 1118–1129, https://doi.org/10.1109/JSEN.2007.897946.
[9] Q. Wang, W.-M. Zhao, A comprehensive review of lossy mode resonance-based fiber optic sensors, Opt. Lasers Eng. 100 (2018) 47–60, https://doi.org/10.1016/j.optlaseng.2017.07.009.
[10] P.S. Pandey, S.K. Raghuwanshi, S. Kumar, Recent Advances in Two-Dimensional Materials-Based Kretschmann Configuration for SPR Sensors: A Review, IEEE Sens. J. 22 (2022) 1069–1080, https://doi.org/10.1109/JSEN.2021.3133007.

[11] R. Bandaru, M. Divagar, S. Khanna, C.G. Danny, S. Gupta, V. Janakiraman, S. V V R, U-bent fiber optic plasmonic biosensor platform for ultrasensitive analyte detection, Sens. Actuators B Chem. 321 (2020) 128463, https://doi.org/10.1016/j.snb.2020.128463.
[12] R. Singh, W. Zhang, X. Liu, B. Zhang, S. Kumar, WaveFlex biosensor: MXene-immobilized W-shaped fiber-based LSPR sensor for highly selective tyramine detection, Opt. Laser Technol. 171 (2024) 110357, https://doi.org/10.1016/j.optlastec.2023.110357.
[13] R. Singh, W. Zhang, X. Liu, B. Zhang, S. Kumar, Humanoid-shaped WaveFlex biosensor for the detection of food contamination, Biomed. Opt. Express 14 (2023) 4660, https://doi.org/10.1364/BOE.500311.
[14] R. Singh, Z. Wang, C. Marques, R. Min, B. Zhang, S. Kumar, Alanine aminotransferase detection using TIT assisted four tapered fiber structure-based LSPR sensor: from healthcare to marine life, Biosens. Bioelectron. 236 (2023) 115424, https://doi.org/10.1016/j.bios.2023.115424.
[15] D. Tosi, M. Shaimerdenova, M. Sypabekova, T. Ayupova, Minimalistic design and rapid-fabrication single-mode fiber biosensors: Review and perspectives, Opt. Fiber Technol. 72 (2022) 102968, https://doi.org/10.1016/j.yofte.2022.102968.
[16] M. Shaimerdenova, T. Ayupova, A. Nugmanova, A. Dauletova, D. Tosi, Polarization-sensitive optical fiber-tip ball resonators for refractive index sensing with optical backscatter reflectometer interrogator, Opt. Fiber Technol. 64 (2021) 102551, https://doi.org/10.1016/j.yofte.2021.102551.
[17] S.C. Warren-Smith, S. Afshar V, T.M. Monro, Theoretical study of liquid-immersed exposed-core microstructured optical fibers for sensing, Opt. Express 16 (2008) 9034, https://doi.org/10.1364/OE.16.009034.
[18] M. Shaimerdenova, T. Ayupova, Z. Ashikbayeva, A. Bekmurzayeva, W. Blanc, D. Tosi, Reflector-less shallow-tapered optical fiber biosensors for rapid detection of cancer biomarkers, J. Light. Technol. 41 (2023) 4114–4122, https://doi.org/10.1109/JLT.2022.3187024.
[19] M. Sypabekova, S. Korganbayev, Á. González-Vila, C. Caucheteur, M. Shaimerdenova, T. Ayupova, A. Bekmurzayeva, L. Vangelista, D. Tosi, Functionalized etched tilted fiber Bragg grating aptasensor for label-free protein detection, Biosens. Bioelectron. 146 (2019) 111765, https://doi.org/10.1016/j.bios.2019.111765.
[20] S. Korganbayev, M. Sypabekova, A. Amantayeva, Á. González-Vila, C. Caucheteur, P. Saccomandi, D. Tosi, Optimization of cladding diameter for refractive index sensing in tilted fiber bragg gratings, Sensors 22 (2022) 2259, https://doi.org/10.3390/s22062259.
[21] M. Olivero, A. Bellone, A. Bano, A. Vallan, G. Perrone, Optical fiber flowmeter based on a single mode-multimode-single mode structure, Front. Sens. 3 (2022), https://doi.org/10.3389/fsens.2022.985963.
[22] Y. Zhang, H. Shibru, K.L. Cooper, A. Wang, Miniature fiber-optic multicavity Fabry–Perot interferometric biosensor, Opt. Lett. 30 (2005) 1021, https://doi.org/10.1364/OL.30.001021.
[23] X. Li, L.V. Nguyen, Y. Zhao, H. Ebendorff-Heidepriem, S.C. Warren-Smith, High-sensitivity Sagnac-interferometer biosensor based on exposed core microstructured optical fiber, Sens. Actuators B Chem. 269 (2018) 103–109, https://doi.org/10.1016/j.snb.2018.04.165.
[24] S. Kazhiyev, A. Abdossova, D. Moldabay, A. Rakhimbekova, W. Blanc, D. Tosi, Semi-distributed interferometers fiber-optic sensors for high-sensitivity refractive index detection: design and sensitivity analysis, Measurement 220 (2023) 113327, https://doi.org/10.1016/j.measurement.2023.113327.
[25] Y. Li, Z. Xu, S. Tan, F. Fang, L. Yang, B. Yuan, Q. Sun, Recent advances in microfiber sensors for highly sensitive biochemical detection, J. Phys. D. Appl. Phys. 52 (2019) 493002, https://doi.org/10.1088/1361-6463/ab3d4e.
[26] A. Xiao, Y. Huang, J. Zheng, P. Chen, B.-O. Guan, An optical microfiber biosensor for ceacam5 detection in serum: sensitization by a nanosphere interface, ACS Appl. Mater. Interfaces 12 (2020) 1799–1805, https://doi.org/10.1021/acsami.9b16702.
[27] Y. Ran, J. Long, Z. Xu, Y. Yin, D. Hu, X. Long, Y. Zhang, L. Liang, H. Liang, B.-O. Guan, Harmonic optical microfiber Bragg grating immunosensor for the accelerative test of cardiac biomarker (cTn-I), Biosens. Bioelectron. 179 (2021) 113081, https://doi.org/10.1016/j.bios.2021.113081.
[28] J. Zhang, Q. Sun, R. Liang, J. Wo, D. Liu, P. Shum, Microfiber Fabry–Perot interferometer fabricated by taper-drawing technique and its application as a radio frequency interrogated refractive index sensor, Opt. Lett. 37 (2012) 2925, https://doi.org/10.1364/OL.37.002925.
[29] J. Hu, E. Song, Y. Liu, Q. Yang, J. Sun, J. Chen, Y. Meng, Y. Jia, Z. Yu, Y. Ran, L. Shao, P.P. Shum, Fiber laser-based lasso-shaped biosensor for high precision detection of cancer biomarker-CEACAM5 in serum, Biosensors 13 (2023) 674, https://doi.org/10.3390/bios13070674.
[30] B. Patiño-Jurado, Y. Cardona-Maya, M. Jaramillo-Grajales, Y.J. Montagut-Ferizzola, J.F. Botero-Cadavid, A label-free biosensor based on E-SMS optical fiber structure for anti BSA detection, Opt. Fiber Technol. 74 (2022) 103116, https://doi.org/10.1016/j.yofte.2022.103116.
[31] L. Chen, Y.-K. Leng, B. Liu, J. Liu, S.-P. Wan, T. Wu, J. Yuan, L. Shao, G. Gu, Y.Q. Fu, H. Xu, Y. Xiong, X.-D. He, Q. Wu, Ultrahigh-sensitivity label-free optical fiber biosensor based on a tapered singlemode- no core-singlemode coupler for Staphylococcus aureus detection, Sens. Actuators B Chem. 320 (2020) 128283, https://doi.org/10.1016/j.snb.2020.128283.
[32] C. Zhou, J. Tian, Y. Yao, Ultrasensitive and wide-measuring-range refractive index sensor with optical path length-tunable vernier effect, IEEE Sens. J. 23 (2023) 24539–24544, https://doi.org/10.1109/JSEN.2023.3309333.
[33] T. Zhu, K. Chah, F. Chiavaioli, J. Villatoro, C. Caucheteur, Gold-coated optical fiber supermode interferometer for insulin bio-sensing, Opt. Laser Technol. 168 (2024) 109878, https://doi.org/10.1016/j.optlastec.2023.109878.
[34] A. Rakhimbekova, K. Seitkamal, B. Kudaibergenov, F. Nazir, T. Pham, W. Blanc, L. Vangelista, D. Tosi, Fiber-optic semi-distributed Fabry-Perot interferometer for low-limit label-free detection of CCL5 cancer biomarker, Opt. Laser Technol. 168 (2024) 109953, https://doi.org/10.1016/j.optlastec.2023.109953.
[35] A.D. Gomes, H. Bartelt, O. Frazão, Optical vernier effect: recent advances and developments, Laser Photon. Rev. 15 (2021), https://doi.org/10.1002/lpor.202000588.
[36] D. Tosi, Simultaneous detection of multiple fiber-optic fabry–perot interferometry sensors with cepstrum-division multiplexing, J. Light. Technol. 34 (2016) 3622–3627, https://doi.org/10.1109/JLT.2016.2575041.
[37] Y. Liu, X. Li, Y. Zhang, Y. Zhao, Fiber-optic sensors based on Vernier effect, Measurement 167 (2021) 108451, https://doi.org/10.1016/j.measurement.2020.108451.
[38] Z. Lu, T. Robine, M. Guzik, M. Bellec, D. Tosi, C. Molardi, F. Pigeonneau, W. Blanc, Shaping nanoparticles in optical fibers through thermal engineering, in: S. Taccheo, M. Ferrari, A.B. Seddon (Eds.), Fiber Lasers Glas. Photonics Mater. through Appl. III, SPIE,, 2022, p. 23, https://doi.org/10.1117/12.2620076.
[39] W. Blanc, Z. Lu, T. Robine, F. Pigeonneau, C. Molardi, D. Tosi, Nanoparticles in optical fiber, issue and opportunity of light scattering [Invited, Opt. Mater. Express 12 (2022) 2635, https://doi.org/10.1364/OME.462822.
[40] W. Blanc, V. Mauroy, L. Nguyen, B.N. Shivakiran Bhaktha, P. Sebbah, B.P. Pal, B. Dussardier, Fabrication of rare earth-doped transparent glass ceramic optical fibers by modified chemical vapor deposition, J. Am. Ceram. Soc. 94 (2011) 2315–2318, https://doi.org/10.1111/j.1551-2916.2011.04672.x.
[41] D. Tosi, C. Molardi, M. Sypabekova, W. Blanc, Enhanced backscattering optical fiber distributed sensors: tutorial and review, IEEE Sens. J. 21 (2021) 12667–12678, https://doi.org/10.1109/JSEN.2020.3010572.
[42] M. Froggatt, J. Moore, High-spatial-resolution distributed strain measurement in optical fiber with Rayleigh scatter, Appl. Opt. 37 (1998) 1735, https://doi.org/10.1364/AO.37.001735.
[43] C. Liang, Q. Bai, M. Yan, Y. Wang, H. Zhang, B. Jin, A comprehensive study of optical frequency domain reflectometry, IEEE Access 9 (2021) 41647–41668, https://doi.org/10.1109/ACCESS.2021.3061250.
[44] K. Karipbayeva, W. Blanc, D. Tosi, Optical fiber semi-distributed interferometer assisted by an FBG for thermorefractometry and sweat sensing, IEEE Sens. J. 23 (2023) 14161–14166, https://doi.org/10.1109/JSEN.2023.3277004.
[45] A.D. Gomes, J. Kobelke, J. Bierlich, J. Dellith, M. Rothhardt, H. Bartelt, O. Frazão, Giant refractometric sensitivity by combining extreme optical Vernier effect and modal interference, Sci. Rep. 10 (2020) 19313, https://doi.org/10.1038/s41598-020-76324-7.
[46] D. Tosi, Review and analysis of peak tracking techniques for fiber bragg grating sensors, Sensors 17 (2017) 2368, https://doi.org/10.3390/s17102368.
[47] J.S. Paiva, P.A.S. Jorge, R.S.R. Ribeiro, M. Balmaña, D. Campos, S. Mereiter, C. Jin, N.G. Karlsson, P. Sampaio, C.A. Reis, J.P.S. Cunha, iLoF: An intelligent Lab on fiber approach for human cancer single-cell type identification, Sci. Rep. 10 (2020) 3171, https://doi.org/10.1038/s41598-020-59661-5.
[48] T. Ayupova, M. Shaimerdenova, M. Sypabekova, L. Vangelista, D. Tosi, Picomolar detection of thrombin with fiber-optic ball resonator sensor using optical backscatter reflectometry, Opt. (Stuttg.) 241 (2021) 166969, https://doi.org/10.1016/j.ijleo.2021.166969.
[49] M. Shaimerdenova, T. Ayupova, M. Sypabekova, D. Tosi, Fiber optic refractive index sensors based on a ball resonator and optical backscatter interrogation, Sensors 20 (2020) 6199, https://doi.org/10.3390/s20216199.